University of Groningen

Passivity-Based Control by Series/Parallel Damping of Single-Phase PWM Voltage Source Converter

del Puerto Flores, Dunstano; Scherpen, Jacqueline; Liserre, Marco; de Vries, Martijn M. J.; Kransse, Marco J.; Monopoli, Vito Giuseppe

Published in:
IEEE Transactions on Control Systems Technology

DOI:
10.1109/TCST.2013.2278781

IMPORTANT NOTE: You are advised to consult the publisher's version (publisher's PDF) if you wish to cite from it. Please check the document version below.

Document Version
Final author's version (accepted by publisher, after peer review)

Publication date:
2014

Link to publication in University of Groningen/UMCG research database

Citation for published version (APA):
del Puerto Flores, D., Scherpen, J., Liserre, M., de Vries, M. M. J., Kransse, M. J., & Monopoli, V. G. (2014). Passivity-Based Control by Series/Parallel Damping of Single-Phase PWM Voltage Source Converter. *IEEE Transactions on Control Systems Technology*, *22*(4), 1310-1322. https://doi.org/10.1109/TCST.2013.2278781

Copyright
Other than for strictly personal use, it is not permitted to download or to forward/distribute the text or part of it without the consent of the author(s) and/or copyright holder(s), unless the work is under an open content license (like Creative Commons).

Take-down policy
If you believe that this document breaches copyright please contact us providing details, and we will remove access to the work immediately and investigate your claim.

Downloaded from the University of Groningen/UMCG research database (Pure): http://www.rug.nl/research/portal. For technical reasons the number of authors shown on this cover page is limited to 10 maximum.

Download date: 26-12-2020

Passivity-Based Control by Series/Parallel Damping of Single-Phase PWM Voltage Source Converter

Dunstano del Puerto-Flores, Jacquelien M. A. Scherpen, Marco Liserre,
Martijn M. J. de Vries, Marco J. Kransse, Vito G. Monopoli

***Abstract*—This paper describes a detailed design procedure for passivity–based controllers developed using the Brayton–Moser framework. Several passivity-based feedback designs are presented for the Voltage-Source Converter, specifically for the H–bridge converter, since nowadays it is one of the preferred solutions to connect direct current (dc) loads or distributed sources to the alternating current (ac) grid. Independent of the operating mode, namely, the rectifier and regenerative operating mode, the achieved control aims are: high power-factor correction in the ac-side and optimal dc voltage regulation capability in the dc-side. The proposed controllers can use series or parallel damping-based solutions for the error dynamics, naturally providing the conditions for stability and tuning of control parameters. Moreover, the Brayton-Moser structure facilitates the addition of virtual RLC filter circuits to the control design for the rejection of low frequency harmonics. The effectiveness of series/parallel damping is investigated in case of abrupt changes in the load, using conductance estimators. Simulation and experimental results validate the analysis.**

***Index Terms*—Passivity-based control, harmonic compensation, load estimation, Brayton-Moser systems, mixed-potential function, tuning rules, voltage source converter, power converters.**

I. Introduction

THE single-phase Voltage Source Converter (VSC), like the H–bridge or full bridge converter, can be used as universal converter due to the possibility to perform dc-dc, dc-ac or ac-dc conversion [1]. Moreover, it can be used as basic cell of the cascade multilevel converters [2] and [3]. Independent of the operating mode, namely the rectifier or regenerative operating mode, the control aims are: high power-factor correction at the ac-side and dc voltage regulation at the dc-side. These objectives should be satisfied, regardless of the conditions of the grid, the dc load/source and the converter nonlinearities.

The control of such power inverter/rectifier converters has been subject of many scientific studies, though conventional linear control techniques are most often applied in practice, see e.g. [3]–[8] and the references therein. Among them, proportional-resonant (PR) controllers and filter-based active damping control achieve the above objectives with small steady-state error and high power factor correction [5], [6]. However, the use of linear techniques require a linearization of the dynamical behavior around the steady-state operating point (or trajectory) and therefore these controllers are suitable in those cases where the converter operates within fixed operating points and the variation of system parameters and disturbances are small. Thus, such controllers only ensure local stability.

The models of power converters are nonlinear since the control signals (the switches) appear in a nonlinear (bilinear) form in the model. Furthermore, there are often nonlinear components present in the converters, e.g. nonlinear loads or/and sources. When the converters are required to function over a wide operating range, linearization is not suitable. For instance, in [9] it is shown that three-phase VSC controlled by regular linear controllers, e.g. cascaded PI's, may become unstable in the regenerative operating mode. Many nonlinear control strategies overcome such problems, both for single-phase and three-phase H–bridge converters, see e.g. [8], [10]–[16] and [9], [17]–[21] respectively. But most of the obtained results for three-phase power inverter/rectifier converters are not directly applicable for single-phase systems, specifically when d-q transformation theory is used [5].

Among the nonlinear control techniques, Passivity-Based Control (PBC) is an important framework for the control of nonlinear systems and widely used for controlling switched-mode power converters, see e.g. [22]. The main advantage of PBC is the explicit use of knowledge of the physical system structure in the controller, e.g. energy, dissipation and interconnection. Therefore, the basic idea behind PBC design is to modify the energy of the system and add damping by modification of the dissipation structure [22]. The PBC approach has been investigated both for single-phase and multilevel configurations although in the majority of cases for the rectifier operating mode [10]–[13], [16]. Also, the bidirectional power flow control of this converter using passive Hamiltonian techniques was studied in [23], but there is still a steady-state error of about $5\ \%$ in the regulated voltage of the dc-side in the regenerative operating mode, due to the lack of harmonics compensation and/or damping injection in the proposed controller.

Based on the Brayton-Moser (BM) framework [24], in [25] a PBC design method which produces a control signal such that the closed-loop dynamics are forced to act as if there are virtual resistors connected in series and/or in parallel to the circuit elements has been presented. These findings were in fact related to the results from [26], where it is shown that the widely used current-mode programming effectively introduces lossless series damping resistance. The BM PBC approach presents advantages over other model based ap-

D. del Puerto-Flores and J.M.A. Scherpen are with the University of Groningen, The Netherlands. Email: j.m.a.scherpen@rug.nl. M. Liserre is with the Christian-Albrechts-University of Kiel, Germany, Email: liserre@gmail.com. V.G. Monopoli is with the Politecnico di Bari, Italy. M.M.J. de Vries and M.J. Kransse contributed to this work when they were with the Delft Center for Systems and Control, Delft University fo Technology, The Netherlands.

proaches, e.g.; a natural description of the dynamics in terms of easily measurable quantities, namely the inductors currents and capacitors voltages; the derived controllers are in terms of dynamic damping of the errors in the controlled variables; and straightforward tuning rules for damping injection. Output voltage regulation by BM-based series/parallel damping injection of the basic buck and boost dc-dc converters and through a pre-compensation scheme to the three-phase ac-dc boost rectifier for load perturbation have been presented in [25] and [27]. respectively. Experimental validations were presented for dc-dc interleaved current-fed full-bridge converter in [28] and for single-phase ac-dc full bridge boost rectifier in [13]. In this paper, unlike the previous cited work, a rigorous stability analysis of the overall system, i.e. the closed loop of the converter with the proposed controllers, is presented.

The aim of this paper is to develop and validate the BM modeling framework for PBC in a systematic way for the H bridge converters. For such converters the obtained controllers indirectly stabilize the dc voltage at the dc-side and directly achieves a unity power-factor at the ac-side. Moreover, the control objectives are achieved during the rectifier and regenerative operating mode. In [27] a PBC is developed for a three phase boost rectifier, but these results are not straightforwardly extended to single-phase systems. Therefore, we include an adaptation scheme in the designs, and robustness of the adaptive PBC design is tested in an experimental set-up. PBC with adaptive scheme was studied previously in [10], [11], however the inductor resistance was neglected and consequently there is a steady error in the input current. Here, it is shown that series-damping injection overcomes this problem.

Furthermore, the problem of grid current harmonic rejection is covered in this paper. This is particularly of interest for single–phase grid connected applications due to the fact that the desired current is a sinusoidal quantity and its tracking is rather demanding [7], [29]. Specifically, a dynamic damping injection scheme for the compensation of harmonic distortion is proposed, see [6], [30] for a related development. Here, we study grid harmonic rejection for the H-bridge converter and it is implemented by means of bandpass filters that filter out selected harmonics of the ac-side current. These filters can be physically interpreted as RLC filters, fitting nicely into the BM framework. The resulting design is also included into the experimental validation we perform.

II. Passivity-Based Control of BM Systems

In order to make this paper self-contained, we briefly present Brayton-Moser systems, and review the passivity and power-balance inequality properties for a class of BM networks, first pointed out in [31].

A. Brayton-Moser Systems as Passive Systems

Consider the BM equations as the gradient system affine in the input

$$Q(x)\dot{x} = \nabla_x \mathcal{P}(x) + g(x)u \tag{1}$$

where $\dot{x} := dx/dt$, $\nabla_x = \partial/\partial x$, $x \in \mathbb{R}^n$, $Q(x) : \mathbb{R}^n \to \mathbb{R}^{n\times n}$ is a full rank matrix containing the incremental inductance and capacitance matrices, $\mathcal{P}(x) : \mathbb{R}^n \to \mathbb{R}$ is the circuit's mixed-potential function (which has the units of power), $g(x)$ the (full rank) input matrix and input signal $u \in \mathbb{R}^m$, $m \leq n$. Stability of a BM system is proven by finding an *alternative pair* $\tilde{Q}(x)$ and $\tilde{\mathcal{P}}(x)$, which equivalently describe (1) and where $\tilde{\mathcal{P}}(x)$ can be used as candidate Lyapunov function, see [24], [32].

Lemma 1: [31] For a given pair $(\mathcal{P}, Q)$ and for any arbitrary constant λ and any smooth symmetric matrix $M(x) \in \mathbb{R}^{n\times n}$, the pair

$$\tilde{Q} = \lambda Q + \tfrac{1}{2}\left(\nabla_x \left(M\nabla_x \mathcal{P}\right) + \nabla_x^2 PM\right) Q, \tag{2}$$

$$\tilde{\mathcal{P}} = \lambda \mathcal{P} + \tfrac{1}{2}\left(\nabla_x \mathcal{P}\right)^\top M \nabla_x \mathcal{P}, \tag{3}$$

where $\nabla_x^2 := \partial^2/\partial x^2$, equivalently characterizes the dynamics (1) as the form

$$\tilde{Q}(x)\dot{x} = \nabla_x \tilde{\mathcal{P}}(x) + \tilde{g}(x)u \tag{4}$$

$$y = -\tilde{g}^\top(x)\dot{x}, \tag{5}$$

where $\tilde{g} = \tilde{Q}Q^{-1}g$ and y is now added as an output.
If the matrix $\tilde{Q}(x)$ satisfies the condition $\tilde{Q}(x) + \tilde{Q}^\top(x) < 0$, then $\tilde{Q}(x)$ is invertible for all $x \in \mathbb{R}^n$. Furthermore, since $\tilde{\mathcal{P}}$ is non-negative, then (4-5) defines a *passive* system with port variables u and y and storage function $\tilde{\mathcal{P}}$, that is,

$$\dot{\tilde{\mathcal{P}}} = \dot{x}^\top(\tilde{Q}(x) + \tilde{Q}^\top(x))\dot{x} + u^\top y \leq u^\top y. \tag{6}$$

The system (4-5), and consequently (1), satisfies the power balance inequality

$$\tilde{\mathcal{P}}(x(t)) - \tilde{\mathcal{P}}(x(0)) \leq \int_0^t u^\top(\tau)y(\tau)d\tau. \tag{7}$$

Remark 2: Lemma 1 and the *power balance inequality* (7) motivated, together with the problem of pervasive dissipation in electrical circuits, the development of the paradigm of power shaping control in [32]. This approach have been recently extended to general nonlinear systems in [33].

B. Passivity-based control through power shaping

In the paradigm of power shaping, as suggested by its name, stabilization is achieved by shaping the power instead of the energy. The starting point of power shaping is a description of the system by BM equations of the form (4-5). By Lemma 1, let us assume that the system equivalently defines a passive system with port variables u and y with respect to the non-negative storage function $\tilde{\mathcal{P}}$, that is,

$$\dot{\tilde{\mathcal{P}}} = \dot{x}^\top(\tilde{Q}(x) + \tilde{Q}^\top(x))\dot{x} + u^\top y \leq u^\top y,$$

where the invertible matrix $\tilde{Q}(x)$ satisfies $\tilde{Q}(x) + \tilde{Q}^\top(x) \leq 0$ for all $x \in \mathbb{R}^n$.

Hence, if $\bar{x}$ is a strict local minimum of $\tilde{\mathcal{P}}$, then $\bar{x}$ is a stable equilibrium point of the unforced system with $u = 0$. In order to stabilize to another point $x^\star$, the mixed-potential function $\tilde{\mathcal{P}}$ is shaped into a nonnegative function having $x^\star$ as a strict local minimum. That is, the control $u = \beta(x)$ where

$$\tilde{g}(x)\beta(x) = \nabla_x \mathcal{P}_a(x),$$

for some $\mathcal{P}_a : \mathbb{R}^n \to \mathbb{R}$, yields the closed-loop system

$$\tilde{Q}(x)\dot{x} = \nabla_x \tilde{\mathcal{P}}_d(x), \tag{8}$$

with total Lyapunov function $\tilde{\mathcal{P}}_d(x) := \tilde{\mathcal{P}}(x) + \mathcal{P}_a(x)$. The new equilibrium will be stable if $x^\star = \arg\min \tilde{\mathcal{P}}_d(x)$.

C. Averaged Mixed-Potential Shaping

Switching power converters are complex hybrid devices that can be represented as switched-BM systems. Such converters are controlled by using a high frequency pulse-width modulation (PWM) technique. Moreover, under the assumption of high frequency operation switched-BM equations can be replaced by its continuous-time averaged approximation models and can be rewritten in the averaged-BM form

$$Q(z)\dot{z} = \nabla_z \mathcal{P}^\mu(z) + g^\mu(z)u, \tag{9}$$

where $-1 \leq \mu \leq 1$ is the duty ratio function and the actual state $x(t)$ is replaced by the average state $z(t)$, see [25] for further details.

Following the PBC methodology of Subsection II-B we will achieve the control objective by making the closed-loop system passive with respect to a desired storage function. Motivated by the form of the average BM system model (9), we propose as desired error dynamics

$$Q\dot{\tilde{z}} + \nabla_{\tilde{z}} \mathcal{P}_d^\mu(\tilde{z}) = \Theta, \tag{10}$$

where $\tilde{z} \triangleq z - \xi$, and ξ the desired value of z, yet to be defined, Θ is the perturbation term, and the desired mixed-potential function satisfies $\mathcal{P}_d^\mu(\tilde{z}) = 0$ always when $\tilde{z} = 0$. This is tantamount to modifying the dissipative voltage and current-potentials associated with the averaged mixed-potential, resulting in a desired error mixed-potential of the form

$$\mathcal{P}_d^\mu(\tilde{z}) = \underbrace{\mathcal{P}_o^\mu(z)|_{z=\tilde{z}}}_{\text{Power shaping}} - \underbrace{(\mathcal{G}_a^\mu(\tilde{z}) - \mathcal{J}_a^\mu(\tilde{z}))}_{\text{Injected damping}}. \tag{11}$$

where $\mathcal{P}_o^\mu(z)$ describes the desired power circulating in the circuit's passive elements, $\mathcal{G}_a^\mu(\tilde{z})$ and $\mathcal{J}_a^\mu(\tilde{z})$ are the added dissipative voltage and current-potentials in terms of the errors, respectively.

Motivated by the Lemma 1, we assume that:

Assumption 3: There exists a constant λ and a matrix $M(\tilde{z})$ in Lemma 1 such that $\tilde{Q}^\mu + (\tilde{Q}^\mu)^\top < 0$, with $\tilde{Q}^\mu$ as in (2) and $\tilde{\mathcal{P}}^\mu \geq 0$ as in (3). The pair $\{\tilde{Q}^\mu, \tilde{\mathcal{P}}^\mu\}$ equivalently characterizes the dynamics (10) as the form

$$\tilde{Q}^\mu \dot{\tilde{z}} + \nabla_{\tilde{z}} \tilde{\mathcal{P}}_d^\mu(\tilde{z}) = \tilde{g}^\mu \Theta, \tag{12}$$

where $\tilde{g}^\mu = \tilde{Q}^\mu (Q^\mu)^{-1}$.
If we set $\Theta \equiv 0$, then the time derivative of $\tilde{\mathcal{P}}_d^\mu$ along (12) is

$$\frac{d\tilde{\mathcal{P}}_d^\mu}{dt} = \frac{1}{2}\dot{\tilde{z}}^\top \left(\tilde{Q}^\mu + (\tilde{Q}^\mu)^\top\right)\dot{\tilde{z}}. \tag{13}$$

Since $\tilde{Q}^\mu + (\tilde{Q}^\mu)^\top < 0$, with $\mu \in [-1, 1]$, then $\dot{\tilde{\mathcal{P}}}_d^\mu \leq 0$. In fact, boundedness of the trajectories and convergence of $z \to \xi$, as $t \to \infty$ can be proven by applying Lasalle's invariance principle.

The associated implicit controller dynamics can be obtained from the perturbation term Θ, which is defined as

$$\Theta := Q\dot{\xi} - \nabla_\xi \mathcal{P}_c^\mu(\xi). \tag{14}$$

where $\mathcal{P}_c^\mu(\xi)$ is the controller mixed-potential function, given by

$$\mathcal{P}_c^\mu(\xi) = \mathcal{P}^\mu(z)|_{z=\xi} + (\mathcal{G}_a^\mu(z-\xi) - \mathcal{J}_a^\mu(z-\xi)). \tag{15}$$

The next step of the design is to obtain, using (14), an explicit expression for the control signal μ, required to assign the desired average mixed-potential function, that is, to ensure that $\Theta = 0$. In the context of model-based PBC designs for power-converters[1], one fundamental question arises:

- Which variables have to be stabilized to a certain value in order to regulate the output(s) of interest toward a desired equilibrium value?

Such a question involves a study of the zero-dynamics yielding either a regulation scheme based on forcing the inductor currents to their desired values or a regulation scheme based on the forcing the capacitor voltages to their desired values.

D. Tuning of the power-based passivity-based control

Damping injection to modify the dissipation structure of the system is an important part of PBC design. In [25] a systematic tool for tuning of various control parameters have been developed based on the BM formulation, instead of the form of the open-loop structure of the system.

Returning to the average BM system model, let $\tilde{i} = \mathrm{col}(\tilde{z}_1, \ldots, \tilde{z}_{n_L})$ and $\tilde{v} = \mathrm{col}(\tilde{z}_{n_L+1}, \ldots, \tilde{z}_{n_L+n_C})$ denote the error-currents through the inductors and error-voltages across the capacitors, and, from (12), consider the unperturbed error dynamics as follows

$$\tilde{Q}\dot{\tilde{z}} - \nabla_{\tilde{z}} \mathcal{P}_d^\mu(\tilde{z}) = 0, \tag{16}$$

with the average desired mixed potential has the form

$$\mathcal{P}_d^\mu(\tilde{z}) = \tilde{i}^\top \Psi(\mu)\tilde{v} + \mathcal{G}_d^\mu(\tilde{i}) - \mathcal{J}_d^\mu(\tilde{v}), \tag{17}$$

where $\mathcal{G}_{\mathrm{d}}^\mu(\tilde{z})$ and $\mathcal{J}_{\mathrm{d}}^\mu(\tilde{z})$ are the modified dissipative voltage and current-potentials in terms of the errors, resp., and the modified error resistance matrices $R_{\mathrm{d}}(\tilde{i})$ and the modified error conductance matrix $G_{\mathrm{d}}(\tilde{v})$ are defined as

$$R_d(\tilde{i}) = \nabla_{\tilde{i}}^2 \mathcal{P}_d^\mu(\tilde{z}) \tag{18}$$

$$G_d(\tilde{v}) = \nabla_{\tilde{v}}^2 \mathcal{P}_d^\mu(\tilde{z}), \tag{19}$$

and the stability theorems, as presented for a class of BM networks in [24] and for non-switching BM networks in [25], are slightly reformulated as follow:

Theorem 4: (**Series damping**) If $R_d(\tilde{i})$ is a symmetric, constant and positive definite matrix, $G_d^\mu(\tilde{v}) + |\tilde{v}^\top \Psi(\mu)| \to \infty$ as $|\tilde{v}| \to \infty$, and

$$\left\| L^{\frac{1}{2}}(\tilde{i}) R_d^{-1} \Psi(\mu) C^{-\frac{1}{2}}(\tilde{v}) \right\| \leq 1 - \delta, \tag{20}$$

[1] See for instance [18], [22] for Euler-Lagrange, [34] for Port-Hamiltonian, and [25] for Brayton-Moser models.

with $0 < \delta < 1$, then for all bounded $|\mu| \in [0,1]$ the solutions of (10) tend to zero as $t \to \infty$[2].

Theorem 5: (**Parallel damping**) If $G_d(\tilde{v})$ is a symmetric, constant and negative definite matrix, $R_d^{\mu}(\tilde{i}) + |\tilde{i}^{\top}\Psi(\mu)| \to \infty$ as $|\tilde{i}| \to \infty$, and

$$\left\| C^{\frac{1}{2}}(\tilde{v}) G_d^{-1} \Psi^{\top}(\mu) L^{-\frac{1}{2}}(\tilde{i}) \right\| \leq 1 - \delta \tag{21}$$

with $0 < \delta < 1$, then for all $|\mu| \in [0,1]$ the solutions of (10) tend to zero as $t \to \infty$.

III. Problem Formulation

In this section the dynamic model of the Voltage Source Converter (VSC) is first presented and, after identifying its desired operation, the control problem that will be solved in this paper is formulated. Finally, a corresponding average BM model of the converter is given.

A. Converter Dynamics

Consider the single–phase VSC topology shown in Fig. 1. The converter is composed in its main part by a complete (two legs) bidirectional bridge.

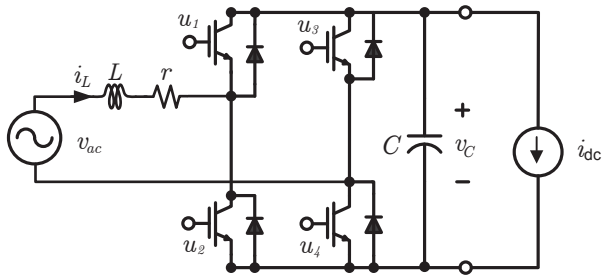

Fig. 1. Single–phase voltage-source converter

The switches in each leg of the converter are complementary operated, i.e., $u_1 = 1 - u_2$ and $u_3 = 1 - u_4$, and, because the switches operate in pairs, $u = u_1 - u_3$ with $u = \{-1, 0, 1\}$. If the switches are controlled with high frequency PWM, then an averaged model can be derived and the parameter u can be replaced by a continuous switching function $\mu \in [-1, 1]$ where $\mu = \mu_1 - \mu_3$ with $\mu_1 \in [0,1]$ and $\mu_3 \in [0,1]$, see [22] for more details. The model describing the averaged behavior of the circuit is given by

$$-L\frac{di_L}{dt} = \mu v_C + r i_L - v_{ac} \tag{22}$$

$$C\frac{dv_C}{dt} = \mu i_L - i_{\rm dc} \tag{23}$$

where i_L is the average inductor current, v_c is the average capacitor voltage, L is the inductance, C is the capacitance, v_{ac} is the voltage of the ac-side grid, with $v_{ac}(t) = E\sin(\omega t)$, r is the parasitic inductor resistance, and $i_{\rm dc}$ is the current at the dc-side. The parameters L, C and r are all assumed to be known constants, where r models dissipation effects in the inductor.

[2]The notation $\|K\|$ denotes the spectral norm of a matrix K, defined as $\|K\|^2 = \max_{|x|=1}\{(Kx)^{\top}Kx\}$.

B. Control Objectives

We deal with the control of the single-phase bidirectional power flow ac-dc converter, namely, the boost-like full bridge converter. The control objectives are formulated as

- **The ac-side**: the converter must be operated with high power factor and zero total harmonic input current, which implies that the desired sinusoidal input current $i_L^{\star}$ should be proportional to the input voltage, i.e., $i_L^{\star} = I_d \sin(\omega t)$. However, for the regenerative operating mode the current i_L and ac voltage $v_{\rm ac}$ must be phase-shifted by 180^o.
- **The dc-side**: the dc-component or the root mean square (RMS) value of the voltage in the dc-side v_C has to be equal to some constant[3] desired value $V_d > E$ in both rectifier and regenerative operating modes.

In [23] it has been shown that a necessary and sufficient condition for the existence of a steady-state regime, i.e., the RMS value of v_C equals to V_d and $i_L^{\star} = I_d \sin(\omega t)$, is that

$$i_{\rm dc} V_d = \tfrac{1}{2}(E - r I_d) I_d, \tag{24}$$

i.e., a power balance must hold. From (24) it can be concluded that the amplitude of the input current, I_d, which corresponds to minimum power that drives the output voltage to the desired level V_d is given by

$$I_d = \frac{E}{2r} - \sqrt{\left(\frac{E}{2r}\right)^2 - \frac{2 i_{\rm dc} V_d}{r}}. \tag{25}$$

Remark 6: As in [23] has been emphasized, a bidirectional flow is allowed since there is no assumption on the sign of $i_{\rm dc} \in \mathbb{R}$, although $i_{\rm dc}$ is considered constant. Furthermore, for given values of E, r, V_d, and with the constraint $V_d > E$ we have that $|i_{\rm dc}| < \frac{E^2}{8 r V_d}$.

C. Averaged-Switched BM Model

The dynamic behavior of the converter system (22-23) can be rewritten in the BM form as follows. Let z_1 and z_2 be the average inductor current, i_L, and the average capacitor voltage, v_C, respectively. If the vector z is defined as $z = [z_1\ z_2]^{\top}$, then the PWM BM equations are defined as

$$-L\dot{z}_1 = \nabla_{z_1}\mathcal{P}^{\mu}(z,t) = \mu z_2 + r z_1 - v_{ac} \tag{26}$$

$$C\dot{z}_2 = \nabla_{z_2}\mathcal{P}^{\mu}(z,t) = \mu z_1 + i_{\rm dc}. \tag{27}$$

For ease of notation, consider the compact form

$$Q(z)\dot{z} - \nabla_z \mathcal{P}^{\mu}(z,t) = 0, \tag{28}$$

where $Q(z) = \mathrm{diag}(-L, C)$. For this power converter it can be shown that the averaged mixed–potential function can be decomposed as

$$\mathcal{P}^{\mu}(z,t) = \mathcal{P}_o^{\mu}(z) + P_s^{\mu}(z,t) \tag{29}$$

[3]As a consequence of the sinusoidal input current, as demonstrated in [17], the output voltage will inevitable have a ripple component with frequency equal to twice the grid frequency. For this reason the control objective is to drive the RMS value of v_C to V_d instead of just the value of v_C.

with the individual terms of the form

$$\mathcal{P}_o^{\mu}(z) = \mu z_1 z_2 + \tfrac{1}{2} r z_1^2, \quad (30)$$

$$\mathcal{P}_s^{\mu}(z,t) = -z_1 v_{ac}(t) + \int_0^{z_2} \hat{i}_{\rm dc}(\tau) d\tau. \quad (31)$$

The term $\mathcal{P}_o^{\mu}(z)$ represents the power circulating across the dynamic elements ($\mu z_1 z_2$), and the dissipative current–potential ($\mathcal{G}(z_1) = \int_0^{z_1} \hat{v}_r(\tau) d\tau = \frac{1}{2} r z_1^2$, with $\hat{v}_r(z_1) = r z_1$ by Ohm's law.) by the current–controlled resistors. The total supplied power by the (input) sources is denoted by $\mathcal{P}_s^{\mu}(z,t)$, i.e., when $\hat{i}_{dc}(t) = i_{dc}$ denotes a constant input current source, then $\mathcal{P}_s^{\mu}(z,t) = -z_1 v_{ac}(t) + i_{dc} z_2$.

IV. Passivity-based controllers for a single-phase AC-DC power converter

In this section we present controllers designed with the PBC approach in the Brayton-Moser framework which have been introduced in [25], [27].

A. Adaptive Passivity-Based Controller

Consider the single–phase Rectifier VSC topology with resistive load. Let z_1 and z_2 represent the averaged inductor current and the averaged capacitor voltage, respectively, and $\mu \in [-1, 1]$. It can be shown that its averaged open-loop mixed-potential is given by

$$P^{\mu}(z,t) = -v_{ac}(t) z_1 + \mu z_1 z_2 + \tfrac{1}{2} r z_1^2 - \tfrac{1}{2} G_\ell z_2^2, \quad (32)$$

which is decomposed as

$$P_o^{\mu}(z) = \mu z_1 z_2 + \tfrac{1}{2} r z_1^2 - \tfrac{1}{2} G_\ell z_2^2, \quad (33)$$

$$P_s(z,t) = -v_{ac}(t) z_1, \quad (34)$$

where $G_\ell = R_\ell^{-1}$. Note that due to the resistive load, now a dissipative voltage–potential ($\mathcal{J}(z_2) = \int_0^{z_2} \hat{i}_g(\tau) d\tau$, with $\hat{i}_g(z_2) = G_\ell z_2$ we have $\mathcal{J}(z_2) = z_2^2 / 2R_\ell$) from the voltage–controlled resistors is added to P_o^{μ} of (30). The respective gradients of (32) yield the corresponding averaged differential equations

$$-L\dot{z}_1 = \nabla_{z_1} \mathcal{P}^{\mu}(z,t) = \mu z_2 + r z_1 - v_{ac} \quad (35)$$

$$C\dot{z}_2 = \nabla_{z_2} \mathcal{P}^{\mu}(z,t) = \mu z_1 - \theta_\ell z_2, \quad (36)$$

where the value of the load $\theta_\ell = G_\ell$ is assumed to be unknown. Therefore, as in [13], [17], an estimator is used to estimate the correct value of G_ℓ. Following the methodology of Subsection II-C, for the converter (35-36), an indirect regulation policy of the output voltage is summarized in the next proposition.

Proposition 7: Consider the switched BM system (35-36), where C, L, $E > 0$ are known constants parameters, and $R_\ell > 0$ is the unknown load resistance but constant. The adaptive nonlinear dynamic feedback PBC controller

$$\mu = \frac{1}{\xi_2}(v_{\rm ac} - r z_1^\star - L\dot{z}_1^\star) \quad (37)$$

$$C\dot{\xi}_2 = \mu z_1^\star - \hat{\theta}_\ell \xi_2 + G_{\rm a} \tilde{z}_2, \quad \xi_2(0) > 0 \quad (38)$$

$$\dot{\hat{\theta}}_\ell = \alpha \xi_2 \tilde{z}_2 \quad (39)$$

where $\tilde{z}_2 = z_2 - \xi_2$, ξ_2 is the controller state and $\hat{\theta}_\ell$ is the estimated value of θ_ℓ, with the dynamical controller initial condition is chosen so that $\xi_2(0) > 0$ and $\hat{\theta}_\ell(0) > 0$. $\tilde{z}_1 = z_1 - z_1^\star$ and $z_1^\star$ is the desired sinusoidal current for the ac-side, and $G_{\rm a}$ verifies

$$G_{\rm a} \geq \frac{\max|\mu|}{1-\delta}\sqrt{\frac{C}{L}} - \hat{\theta}_\ell, \quad \delta \in (0,1). \quad (40)$$

Under these conditions, the controller solves the tracking problem for the ac-side, i.e. $\lim_{t\to\infty} z_1 = z_1^\star$ and for the dc-side indirectly stabilizes the RMS value of z_2 to V_d.

Proof: Let, again, $z - \xi$ stand for the error vector $\tilde{z}$. In terms of the error signals (35–36) are rewritten as,

$$Q\dot{\tilde{z}} + \nabla \mathcal{P}_o^{\mu}(z)|_{z=\tilde{z}} = \Theta \quad (41)$$

The controller dynamics is determined by taking the respective gradients of the controller mixed potential

$$\mathcal{P}_c^{\mu}(\xi, z, t) = \mathcal{P}^{\mu}(z,t)|_{z=\xi} + \tfrac{1}{2} r_{\rm a}(z_1 - \xi_1)^2 - \tfrac{1}{2} G_{\rm a}(z_2 - \xi_2)^2, \quad (42)$$

by replacing G_ℓ with $\hat{\theta}_\ell$, indeed the controller is implicitly described by

$$-L\dot{\xi}_1 = -v_{\rm ac} + \mu \xi_2 + r\xi_1 - r_{\rm a}(z_1 - \xi_1) \quad (43)$$

$$C\dot{\xi}_2 = \mu z_1^\star - \hat{\theta}_\ell \xi_2 + G_{\rm a}(z_2 - \xi_2), \quad (44)$$

Substraction of (43–44) from (35–36) yields the following perturbed error dynamics, i.e.,

$$-L\dot{\tilde{z}}_1 = \mu \tilde{z}_2 + (r + r_{\rm a})\tilde{z}_1 \quad (45)$$

$$C\dot{\tilde{z}}_2 = \mu \tilde{z}_1 - (\theta_\ell + G_{\rm a})\tilde{z}_2 + \tilde{\theta}_\ell \xi_2, \quad (46)$$

where the term $\tilde{\theta}_\ell$ now appears in the above equations and the estimation error is defined as $\tilde{\theta}_\ell = \hat{\theta}_\ell - \theta_\ell$. In order to increase the stability margin, $\hat{\theta}$ is forced to be positive and bounded away from zero and to make sure that the perturbation term $\tilde{\theta}_\ell \xi_2$ converges to zero the parameter update law is chosen to be, as suggests in [17],

$$\dot{\hat{\theta}}_\ell = -{\rm Proj}(\tau) = \begin{cases} \tau = \alpha \tilde{z}_2 \xi_2, & \hat{\theta}_\ell > \epsilon \\ \tau = 0, & \text{otherwise} \end{cases} \quad (47)$$

where $\alpha > 0$ is the adaptive gain and $\epsilon > 0$ with ϵ an arbitrarily small constant.

To prove stability of the error system, consider the following Lyapunov function

$$\mathcal{H}_{\rm ea}^\star(\tilde{z}, \tilde{\theta}_\ell) = \frac{1}{2} L \tilde{z}_1^2 + \frac{1}{2} C \tilde{z}_2^2 + \frac{1}{2\alpha} \tilde{\theta}_\ell^2, \quad (48)$$

where the time derivative along the trajectories of (45–46), and (47) is given by

$$\dot{\mathcal{H}}_{\rm ea}^\star = -(r + r_{\rm a})\tilde{z}_1^2 - (\theta_\ell + G_{\rm a})\tilde{z}_2^2 \leq -\frac{\gamma}{2}\{L\tilde{z}_1^2 + C\tilde{z}_2^2\} \quad (49)$$

with $\gamma = 2\min\{r + r_{\rm a}, G_\ell + G_{\rm a}\} / \max\{L, C\}$. Because $\mathcal{H}_{\rm ea}^\star$ is nonincreasing, $\tilde{z}$ and $\tilde{\theta}_\ell$ are globally uniformly bounded, i.e., $\tilde{z} \in \mathcal{L}_\infty^2$ and $\tilde{\theta}_\ell \in \mathcal{L}_\infty$. In addition, since $\mathcal{H}_{\rm cl}^\star$ is bounded from below by zero, then $\tilde{z}$ is square integrable, i.e., $\tilde{z} \in \mathcal{L}_2^2$. For the use of the LaSalle-Yoshizawa theorem [35], in order to conclude that $\tilde{z}(t) \to 0$ as $t \to \infty$, it must be verified that $\tilde{z}$ is uniformly continuous. For this, by Barbalat's lemma [35],

it is sufficient to show that $\dot{\tilde{z}}$ is bounded.
First, let us assume that $\xi_2(t)$ is bounded away from zero. From the perturbed error dynamics (45–46), and the established boundedness of $\tilde{\theta}$ and $\tilde{z}$, it follows that $\dot{\tilde{z}}$ is bounded if and only if ξ_2 is bounded. In order to prove that ξ_2 is bounded, we evaluate (43-44) in $\xi_1 = z_1^\star$ and solve (43) for μ, where the dynamic controller is defined by

$$\mu = \frac{1}{\xi_2}(v_{\rm ac} - r z_1^\star - L\dot{z}_1^\star) \tag{50}$$

$$C\dot{\xi}_2 = \mu z_1^\star - \hat{\theta}_\ell \xi_2 + G_a \tilde{z}_2, \quad \xi_2(0) > 0 \tag{51}$$

where $r_{\rm a} = 0$ and $z_1^\star = I_d \sin(\omega t)$ with the desired current amplitude of the form

$$I_d = \frac{E}{2r} - \sqrt{\left(\frac{E}{2r}\right)^2 - \frac{2}{r}\left(\hat{\theta}_\ell V_d^2\right)} \tag{52}$$

and, because $\hat{\theta}_\ell$ is forced to be positive and bounded away from zero, we have that $I_d \in \mathcal{L}_\infty$ which implies that $z_1^\star \in \mathcal{L}_\infty$. The time derivative of $\dot{z}_1^\star$ is given by

$$\dot{z}_1^\star = \omega I_d \cos(\omega t) - \frac{2\alpha \tilde{z}_2 \xi_2 V_d^2}{\sqrt{E^2 - 8r(V_d^2 \hat{\theta}_\ell)}} \sin(\omega t).$$

where we easily see that $\dot{z}_1^\star \in \mathcal{L}_\infty$, by the assumption of $\xi_2(t)$ is bounded away from zero. Consequently, since μ depends only on bounded signals, given by (50), this implies that $\mu \in \mathcal{L}_\infty$, and, from (45), it concludes that $\dot{\tilde{z}}_1 \in \mathcal{L}_\infty$, where we used the fact that $\tilde{z}_1, \hat{\theta}_\ell \in \mathcal{L}_\infty$. As $\tilde{z}_1 \in \mathcal{L}_2$ and by Barbalat's lemma [35], we have that $\lim_{t\to\infty} \tilde{z}_1 = 0$.
Since by construction $\hat{\theta}$ is bounded away from zero and from the previous result that $\mu \in \mathcal{L}_\infty$, we can infer that (51) is in fact a first-order system which is input-to-state stable because $\hat{\theta}$ is bounded away from zero. Therefore, we can state that $\xi_2 \in \mathcal{L}_\infty$, which implies that $\dot{\tilde{z}}_2 \in \mathcal{L}_\infty$. Then, we conclude that $\lim_{t\to\infty} \tilde{z}_2 = 0$

Furthermore, by using Theorem 5, we can state from the set of equations (45–46) that $\lim_{t\to\infty} \tilde{z} = 0$, that is $\lim_{t\to\infty} z = \xi$, is satisfied if we set $G_{\rm a}$ as (40) with tuning parameter $\delta \in (0,1)$ and $r_{\rm a} = 0$. ■

Remark 8: An analogous result to (40) can be found for series damping by using Theorem 4, i.e., a lower bounded on $r_{\rm a}$ to ensure non-oscillatory behavior is given by

$$r_{\rm a} > \frac{\max|\mu|}{1-\delta}\sqrt{\frac{L}{C}} - r, \tag{53}$$

with the tuning parameter $\delta \in (0,1)$, and $G_{\rm a} = 0$.
Practical results of this adaptive controller are shown in Subsect. VI-A.

Remark 9: Consider the switched BM system (26-27) depicted in Fig. 1. Instability, in the form of oscillations, of the dc-link voltage can occur when the current source in the dc-side $i_{\rm dc}(t)$ is replaced by a constant power load (CPL). Several loads such as electric motor, actuators, and power electronic converters, when they are well controlled, behave as CPLs at the input terminals. Namely, an increase in the voltage of CPL will result in a decrease in the current, and viceversa. To avoid impracticalities and singularities in the dynamical model, consider the following constant power load:

$$i_{\rm dc}(t) = \begin{cases} \frac{P_\ell}{v_C}, & \text{if} \epsilon_0 \le |v_c| \le 1/\nu_0, \\ 0 & \text{if } |v_c| < \epsilon_0, \end{cases} \tag{54}$$

for some small positive numbers ϵ_0, ν_0, and P_ℓ is considered constant. Stability of the converter (26-27) is analyzed by using Lemma 1, which amounts to proving that $|u| < 1$ is bounded. Lemma 1, by selecting $M = \text{diag}(L^{-1}, C^{-1})$ and $\lambda = r/L$, yields that if

$$r\frac{C}{L} > \frac{P_\ell}{z_2^2}, \tag{55}$$

then (26-27) defines a passive system. Moreover, for given values of P_ℓ, L, r and $z_2^\star$, we can use (55) in order to size the dc capacitor. Similar conditions can be found by means of linearization and small-signal analysis [36], [37]. Numerical results show that the adaptive passivity-based control of Proposition 7 ensures that the dc-link voltage v_c is following its reference V_d with CPL.

B. Passivity-Based Controller for a Bidirectional power flow

In this section we present a controller that indirectly stabilizes the average constant voltage in the dc-side and directly achieves a unity power factor on the ac-side during the rectifier and regenerative operating mode.

Proposition 10: Consider the switched BM system (26–27), in closed-loop with the PBC controller

$$\mu = \frac{1}{\xi_2}(v_{\rm ac} - r z_1^\star - L\dot{z}_1^\star + r_{\rm a}\tilde{z}_1) \tag{56}$$

$$C\dot{\xi}_2 = -\mu z_1^\star + \frac{1}{\kappa}(V_d - \xi_2) - i_{\rm dc}, \tag{57}$$

where ξ_2 is the state of the controller, $\tilde{z}_1 = z_1 - z_1^\star$ and $z_1^\star$ is the desired sinusoidal current for the ac-side, V_d is the desired voltage for the dc-side, κ is a positive scalar, and $r_{\rm a}$ verifies

$$r_{\rm a}(\mu) = \frac{1}{1-\delta}\sqrt{\frac{\mu^2 L}{C}} - r.$$

Under these conditions, the controller solves the tracking problem for the ac-side, that is, $\lim_{t\to\infty} z_1 = z_1^\star$ and for the dc-side stabilizes the RMS value of z_2 to V_d.

Proof: The controller dynamics is determined by making a copy of the system in Brayton–Moser form (26–27) in terms of ξ plus an additional damping term, $\mathcal{P}_{\rm a}$. Then, it follows that the controller dynamics is described by

$$Q\dot{\xi} = \nabla_\xi \mathcal{P}^\mu(\xi) + gu + \Lambda \nabla_\xi \mathcal{P}_{\rm a}(\xi). \tag{58}$$

where $\Lambda = \text{diag}(-1, 1)$. To shape the mixed potential function ξ_1 is restricted to $z_1^\star = I_d \sin(\omega t)$ such that the current of the ac-side of (58) is proportional to $v_{\rm ac}$. Recall that the design goal on the dc-side of (58) is to achieve regulation of the RMS value of ξ_2 to V_d, which is achieved by modifying the dissipation structure and adding a parallel damping term to the controller, in order to ensure asymptotic stability. For the particular case of the single-phase converter, we choose the injected dissipation quadratic in ξ_2 as

$$\mathcal{P}_{\rm a}(\xi_2) = \frac{1}{2\kappa}(V_d - \xi_2)^2. \tag{59}$$

with $\kappa > 0$ and V_d is the desired RMS voltage for the state ξ_2 such that the power on the dc-side of (58) is $\langle p_{\rm dc}(t)\rangle_{dc} = V_d i_{\rm dc} + V_d^2/\kappa$. Then, the dynamic controller is given by

$$-L\dot{z}_1^\star = \mu\xi_2 + rz_1^\star - v_{\rm ac} \quad (60)$$

$$C\dot{\xi}_2 = -\mu z_1^\star + \frac{1}{\kappa}(V_d - \xi_2) - i_{\rm dc}, \quad (61)$$

where the term κ is interpreted as the parallel damping injection term acting on the voltage error in the controller. Then, the control action is obtained after solving (60) for μ with respect to the minimum phase state $z_1^\star$, that is,

$$\mu = \frac{1}{\xi_2}(v_{\rm ac} - rz_1^\star - L\dot{z}_1^\star), \quad (62)$$

where $\xi_2(t) > 0$ for all $t \geq 0$.

Stability of the controller is analyzed by using Lemma 1, which amounts to proving that ξ_2 is bounded. Then, an *admissible* pair $(\tilde{\mathcal{P}}, \tilde{Q})$ is obtained with $M = {\rm diag}(L^{-1}, C^{-1})$ and $\lambda = -r/L + 1/\kappa C$ and it can be shown that

$$\tilde{Q} = \begin{bmatrix} -\frac{1}{2}\left(\frac{L}{C\kappa} + r\right) & \mu \\ -\mu & -\frac{1}{2}\left(\frac{rC}{L} + \frac{1}{\kappa}\right) \end{bmatrix} \quad (63)$$

where $\tilde{Q} + \tilde{Q}^\top < 0$ holds provided that $\kappa > 0$ for all $\xi = [z_1^\star, \xi_2]$. $\tilde{P}$ is given by

$$\tilde{\mathcal{P}} = \frac{1}{4C}\left(\mu z_1^\star - \frac{\xi_2}{\kappa}\right)^2 + \frac{1}{4L}(\mu\xi_2 + rz_1^\star)^2 + \frac{r + \kappa\mu^2}{4\kappa L}\xi_2^2 + \frac{r - \kappa\mu^2}{4\kappa C}\mu z_1^{\star 2}. \quad (64)$$

Therefore, using (63–64) we can find an equivalent dynamics of (60–61) and, since $\tilde{\mathcal{P}} > 0$, by Lemma 1 the dynamics defines a passive systems with port variables $u = [v_{\rm ac}, i_{\rm dc} - V_{\rm dc}/\kappa]$ and $y = -\tilde{Q}Q^{-1}g\dot{\xi}$ with $g = {\rm diag}(-1, -1)$. Then (60–61) is stable and $\xi_2, \dot{\xi}_2 \in \mathcal{L}_\infty$. Moreover, from the power balance of (60–61), as (24) in Subsect. III-B, we have that $\kappa < V_d/i_{\rm dc}$.

Let the average state error vector be defined as $\tilde{z} = z - \xi$. The difference between the state variables of the systems (22-23) and (60–61) defines the error dynamics

$$-L\dot{\tilde{z}}_1 = \mu\tilde{z}_2 + r\tilde{z}_1$$

$$C\dot{\tilde{z}}_2 = \mu\tilde{z}_1 - \frac{1}{\kappa}\tilde{\xi}_2,$$

where $\tilde{\xi}_2 = V_d - \xi_2$. In order to ensure non-oscillatory convergence of the error state, damping is added to the state, see [25]. Therefore, consider the injected dissipation quadratic in $\tilde{z}_1$ as

$$\mathcal{G}_{\rm a}(\tilde{z}_1) = \frac{r_{\rm a}}{2}\tilde{z}_1^2. \quad (65)$$

with $r_{\rm a} > 0$. Then, the error dynamics is given by

$$-L\dot{\tilde{z}}_1 = \mu\tilde{z}_2 + (r + r_{\rm a})\tilde{z}_1 \quad (66)$$

$$C\dot{\tilde{z}}_2 = \mu\tilde{z}_1 - \frac{1}{\kappa}\tilde{\xi}_2. \quad (67)$$

Again, by using Lemma 1, with $M = {\rm diag}(2/r_s, 0)$, $r_s = r + r_{\rm a}$, and $\lambda = -1$, it can be shown that

$$\tilde{Q} = \begin{bmatrix} -L & 0 \\ -\frac{2\mu L}{r_s} & -C \end{bmatrix} \quad (68)$$

where $\tilde{Q} + \tilde{Q}^\top < 0$ holds provided that

$$1 > \frac{\mu}{r_s}\sqrt{\frac{L}{C}}. \quad (69)$$

for all $\tilde{z}$. And $\tilde{P}$ is given by

$$\tilde{P}^\mu(\tilde{z}) = \frac{1}{2r_s}(r_s\tilde{z}_1 + \mu\tilde{z}_2)^2 + \frac{1}{2r_s}\mu^2\tilde{z}_2^2, \quad (70)$$

which is strictly positive, with minimum of $\tilde{P}^\mu$ is $\tilde{z} = 0$, then (66-67) defines a passive system with the input $\tilde{\xi}_2 \in \mathcal{L}_\infty$ and the output $\dot{\tilde{z}}_2$. Furthermore, since the RMS of $\xi_2 \to V_d$ and the average of $\tilde{\xi}_2$ equals to zero, then the equilibrium $\tilde{z} = 0$ of (66-67) is stable (see e.g., [38]).

Moreover, from (69) we have that the lower bound for the series damping injection strategy is given as

$$r_{\rm a}(\mu) = \frac{1}{1 - \delta}\sqrt{\frac{\mu^2 L}{C}} - r \qquad G_{\rm a}(\mu) = 0 \quad (71)$$

with tuning parameter $\delta \in (0, 1)$, as it was pointed out in [25].

Finally, it follows that the controller is given as (56-57). ■

C. Numerical results

Simulations are performed of the closed-loop behavior of a boost full-bridge converter in the rectifier and regenerative operating modes by means of the power-based indirect PWM controller (56-57). The parameters that are used for simulation are the same of the experimental setup of the next section and are given in Table I. Control parameters have been selected as follows: the tuning parameter of the series damping, $\delta = 0.5$, the gain of the parallel damping, $\kappa = 0.05$, and the initial conditions $z_1(0) = 0$, $z_2(0) = \xi_2(0) = 10V$.

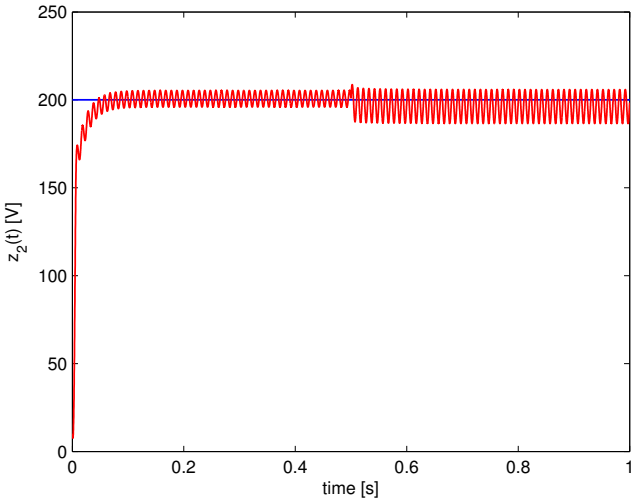

Fig. 2. Simulated response of the capacitor average voltage z_2 (red), with the desired dc-bus voltage $V_d = 200$ V (blue).

Fig.2 shows transient responses of the dc voltage z_2 for a sudden change from rectifying to regenerating operation, i.e., the dc-load current varies from $i_{\rm dc} = 1A$ to $-2A$ at $t = 0.5$ sec. Notice the steady state error is about 1 %, which is less than the steady state errof of 5% in [23], where an energy

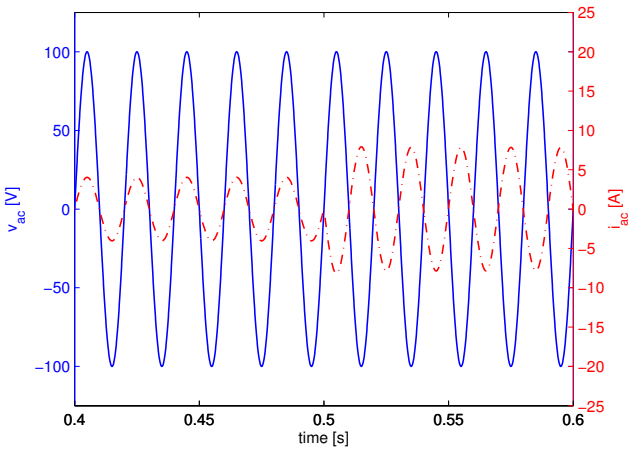

Fig. 3. Source voltage $v_{\rm ac}$ (blue) and current z_1 (red) waveforms

balancing controller is employed. The ac voltage and current are depicted in Fig. 3, where the current waveform shows a 180° phase shift, at $t = 0.5$ sec., as the converter changes from inverter to rectifier mode of operation.

Remark 11: The experimental implementation of the controller (56-57) requires a current load sensor and line side voltage and current sensors. Developing sensorless control strategies is thus important, see for instance [39]. Therefore, realization of bidirectional power control with a reduced number of sensors is currently being studied.

V. Current Shape Improvement

As experienced in practice, the input current of the converter contains higher harmonics. In this section we extent the previous results to meet the design specifications where k current harmonics have to be reduced in amplitude.

A. Harmonics Rejection Problem Formulation

The input current of the single–phase AC–DC boost converter contains harmonics due to internal causes (non–ideal transistors and diodes, blanking times and saturation in the grid–side inductor) and external causes (grid harmonics). Although the internal causes have not been considered for the design of the PBC, these controllers naturally cope with such causes, see [22]. The external causes may result in harmonic distortion and a low power factor. To deal with that, the current shape has to be improved. Without redesigning the converter and inspired by the preliminary results in [40], a passivity–based controller that is based on the frequency domain description of periodic disturbances can accomplish this. Theoretically, an arbitrary number of current harmonics can be reduced by including bandpass filters in the controller where the resonant frequency of each filter coincides with a current harmonic to be reduced in amplitude. These bandpass filters are regarded as damping injection filters and they can be implemented as passive RLC networks.

The mathematical derivation of a passivity–based controller with bandpass filters to compensate for current harmonics follows.

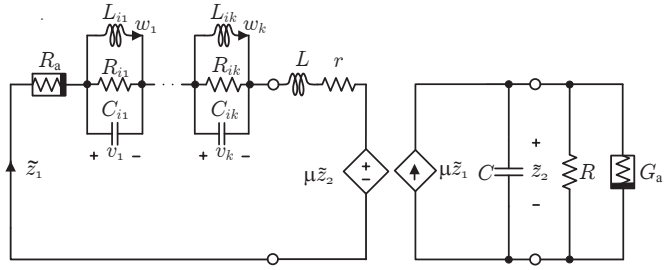

Fig. 4. Schematic interpretation for error dynamics of the power converter with k bandpass filters and virtual series and parallel damping.

B. An Adaptive Passivity-Based Harmonic Controller

The desired error representation is shown in Fig. 4. It is assumed that k current harmonics have to be reduced and the desired error dynamics are formulated as

$$
\begin{aligned}
-L\dot{\tilde{z}}_1 &= \mu\tilde{z}_2 + (r + r_{\rm a})\,\tilde{z}_1 + \sum_{h=1}^{k} v_h && (72)\\
C\dot{\tilde{z}}_2 &= \mu\tilde{z}_1 - (\theta_\ell + G_{\rm a})\tilde{z}_2 + \tilde{\theta}_\ell\xi_2 && (73)\\
L_{i_h}\dot{w}_h &= v_h && (74)\\
C_{i_h}\dot{v}_h &= -w_h - \tfrac{1}{R_{i_h}}v_h + \tilde{z}_1, && (75)
\end{aligned}
$$

where the latter two equations describe the dynamics of the hth bandpass filter, with $h \in \{1, \cdots, k\}$. Notice the value of the load G_ℓ is assumed unknown and a load estimator θ_ℓ is added. Indeed, if the estimator dynamics is chosen as (47), with the Lyapunov function

$$
\mathcal{H}^\star_{\rm ea} = \tfrac{1}{2}(L\tilde{z}_1^2 + C\tilde{z}_2^2) + \tfrac{1}{2}\sum_{h=1}^{k}(L_{ih}w_h^2 + C_{ih}v_h^2) + \frac{1}{2\alpha}\tilde{\theta}_\ell^2, \quad (76)
$$

then it can be proved that $[\tilde{z}, v, w, \tilde{\theta}_\ell]^\top = 0$ is asymptotically stable. To actually obtain the desired error dynamics, based on the previous result of Subsection IV-A, the following controller is used:

$$
\begin{aligned}
\mu &= \frac{1}{\xi_2}\left(v_{\rm ac} - L\dot{z}_1^\star - rz_1^\star + r_{\rm a}\tilde{z}_1^\star + \sum_{h=1}^{k} v_h\right) && (77)\\
C\dot{\xi}_2 &= \mu z_1^\star - \theta_\ell\xi_2 + G_{\rm a}\tilde{z}_2 && (78)\\
\dot{\hat{\theta}}_\ell &= \alpha\xi_2\tilde{z}_2 && (79)\\
L_{i_h}\dot{w}_h &= v_h && (80)\\
C_{i_h}\dot{v}_h &= -w_h - \frac{1}{R_{ih}}v_h + \tilde{z}_1 && (81)
\end{aligned}
$$

with $z_1^\star = I_d\sin(\omega t)$ and I_d as described in (52), $h \in \{1, \cdots, k\}$ and $\xi_2(0) > 0$.

C. Damping Injection Filter Design

It can be verified that the transfer function $T_{ih}(s)$ of each damping injection filter can be described by

$$
T_{ih}(s) = \frac{V_{i_h}(s)}{\tilde{Z}_1(s)} = \frac{\frac{1}{C_{i_h}}s}{s^2 + \frac{1}{R_{i_h}C_{i_h}}s + \frac{1}{L_{i_h}C_{i_h}}}, \quad (82)
$$

where $V_{i_h}(s)$, $\tilde{Z}_1(s)$ denote the Laplace transform of $v_{i_h}(t)$ and $\tilde{z}_1(t)$, respectively, and the parameters L_{i_h}, R_{i_h} and C_{i_h}

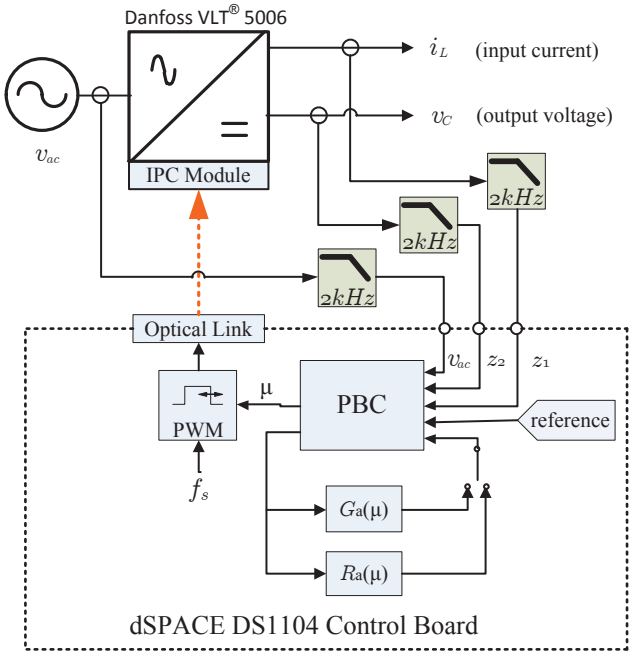

Fig. 5. Scheme of the experimental set-up

are related to important properties of the filter, namely, the resonant frequency ($\omega_0 = 1/\sqrt{L_{i_h} C_{i_h}}$ [rad/s]), the bandwidth ($B = 1/R_{i_h} C_{i_h}$ [rad/s]), and the filter gain at ω_0 ($K = R_{i_h}$ [V/A]).

In general, the values of these parameters are not known a priori. This means that the spectrum of the input current has to be examined and based on this spectrum it has to be decided which frequencies have to be compensated for. In other words, the eigenfrequencies of the filters are fixed. The bandwidth of each filter should be chosen small but large enough to allow deviations in the input frequency. However, the gains of the filters should be chosen reasonably large to suppress the frequencies to be compensated for. This damping injection filter design approach is experimentally tested in Sect. VI.

VI. Experimental Results

In this section the results of load variation experiments and the effects of harmonic compensation are discussed. A diagram of the experimental set–up is schematically shown in Fig. 5. The converter that is used for the experiments is the Danfoss VLT 5006. This is a commercial three–phase rectifier/inverter combination, but in this case the converter is modified and it is used as a single–phase boost converter by using only two switching legs of the inverter.

The parameters of the system are given in Table I. The power dissipation in the converter is modeled by means of a parasitic resistor with resistance r. Since this value cannot be measured it is chosen in such a way that the RMS value of the output voltage and the RMS value and phase of the input current are as desired. For the set–up this value is chosen to be equal to $r = 2.5\ \Omega$.

The original Interface and Protection Card (IPC) is replaced with an IPC developed by the Aalborg University

TABLE I
Parameters values for the experimental setup

Parameter				
Input voltage amplitude	E	=	100	[V]
Input voltage frequency	$\omega/2\pi$	=	50	[Hz]
Capacitance	C	=	340	[μF]
Inductance	L	=	10	[mH]
Parasitic resistance	r	≈	2.5	[Ω]
PWM frequency	f_s	=	12.8	[kHz]
Desired output voltage	V_d	=	200	[V]
Nominal load	R_ℓ	=	220	[Ω]

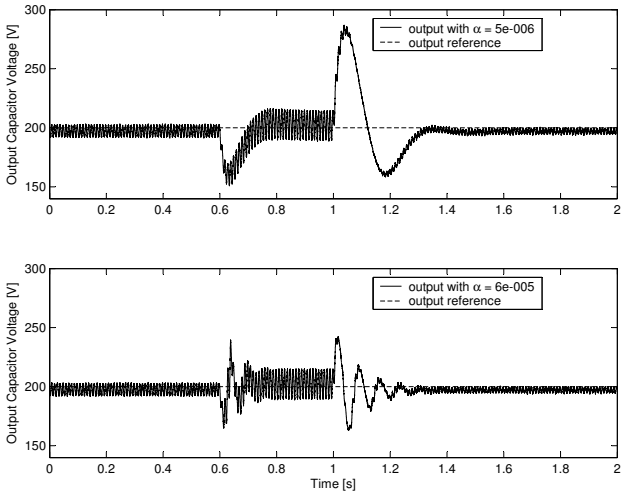

Fig. 8. Output voltage z_2 for the series damping injection scheme during the step–wise load variation, using a low (top plot) and high (bottom plot) adaption gain.

to provide external control over the gate signals. This IPC is optically driven by a dSPACE DS1104 board, where the control algorithm is implemented using the C-code generated by the Real-Time Workshop Target Simulink Library. To prevent aliasing the feedback signals, namely input-current, -voltage, and output voltage, are filtered with first order lowpass filters with cut-off frequencies of 2 kHz. The lowpass filtered signals are sampled at 12.8 KHz by the dSPACE system and consequently, an even number of 256 samples is obtained in one fundamental period of 0.02 s. By choosing an even number some unwanted phenomena (e.g., low frequency oscillations in the output voltage) are avoided. Furthermore, the sampling of the dSPACE system is synchronized with the generation of the pulse width modulated signals. For each leg only one control signal is needed, because the complementary control signal of the second IGBT is generated by the IPC itself. A dead–time of 2 μs is taken into account.

A. Robustness to Load Variation

The controller as described in Sect. IV-A is implemented and connected to the converter. Justified by the tuning rules only one type of damping injection is used at the same time i.e., either (20) or (21). Two different adaption gains are used and the adaption gains are chosen by observing the

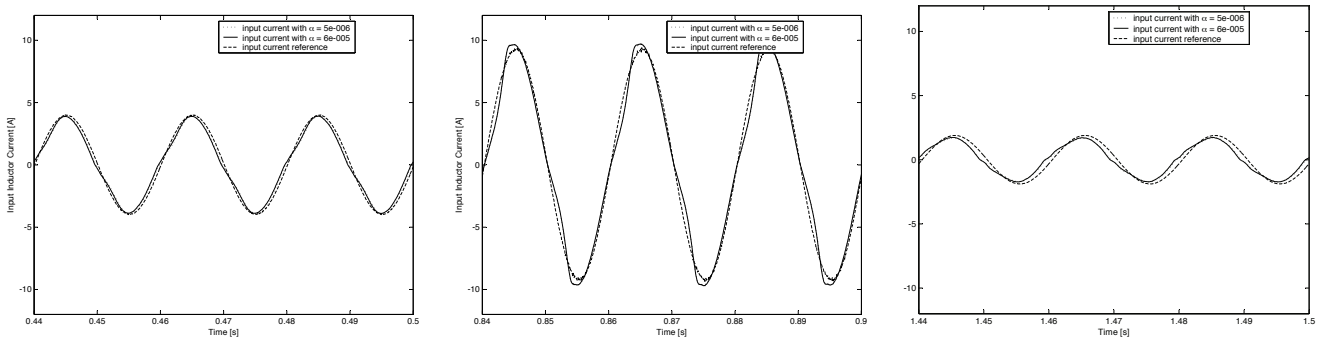

(a) z_1 when $G = \frac{1}{220}\Omega^{-1}$ (b) z_1 when R_ℓ decreases from 100% to 50% (c) z_1 when R_ℓ increases from 100% to 200%

Fig. 6. Input current z_1 for the series damping injection scheme during the step–wise load variation, zoomed in at steady state, using a low (dotted) and high (solid) adaption gain. In steady state the current waveform is not noticeably depending on the value of the adaption gain.

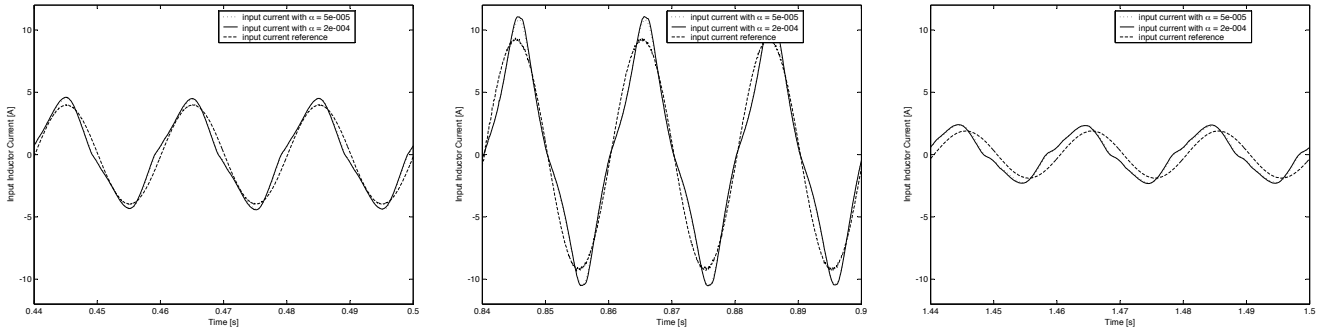

(a) z_1 under nominal $R_\ell = 220\Omega$ (b) z_1 when R_ℓ decreases from 100% to 50% (c) z_1 when R_ℓ increases from 100% to 200%

Fig. 7. Input current z_1 for the parallel damping injection scheme during the step–wise load variation, zoomed in at steady state, using a low (dotted) and high (solid) adaption gain. In steady state the current waveform is not noticeably depending on the value of the adaption gain.

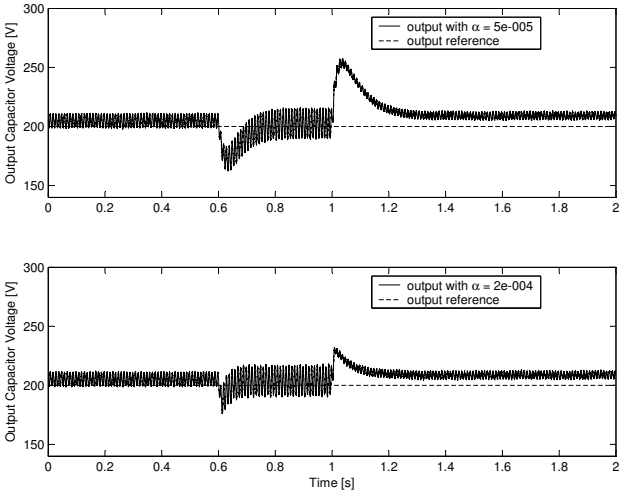

Fig. 9. Output voltage z_2 for the parallel damping injection scheme during the step–wise load variation, using a low (top plot) and high (bottom plot) adaption gain.

converter output. The high adaption gain in the experiments is approximately 80% of the adaption gain that causes the system to behave in an undesired way e.g., causing undesired oscillatory behavior or an over–current through the switches. The low adaption gain is chosen by evaluating the response of the system. In practice, this approach results in different adaption gain values for the series and parallel damping injection schemes.

For the testing of the robustness, the converter is operating with nominal load resistance $R_\ell = 220\ \Omega$ during $0 < t \leq 0.6\ s.$, then R_ℓ is decreased from 100% to 50% (to 110 Ω) during $0.6 < t \leq 1\ s.$, and, finally, R_ℓ is increased from 100% to 200% (to 440 Ω) during $1 < t \leq 2$ s.

1) Series Damping Injection: For this strategy, the damping injection is described by (53). In theory the steady state behavior does not depend on the value of the tuning parameter δ. In addition, (53) only provides a lower bound. Nevertheless, the damping is usually chosen close to the bound. Often the value $\delta = 0.5$ is chosen. In practice however, for low damping values the input current is not sinusoidal and therefore the tuning parameter value is increased to $\delta = 0.9$. The input current z_1 and the output voltage z_2 during the load changes are shown in Fig. 6 and Fig. 8, respectively. In the results the 100 Hz ripple in the output voltage is clearly visible. The amplitude of this ripple depends on the system parameters and, as a consequence, on the load as well. During the variation in the load the RMS value of the output voltage returns to the desired output voltage within a boundary of 2%. From (79) it is clear that the load estimator dynamics depends on the error in the output voltage $\tilde{z}_2$. Since this error is not damped the output of the estimator (not shown here for reasons of space) shows an oscillatory response. When the adaption

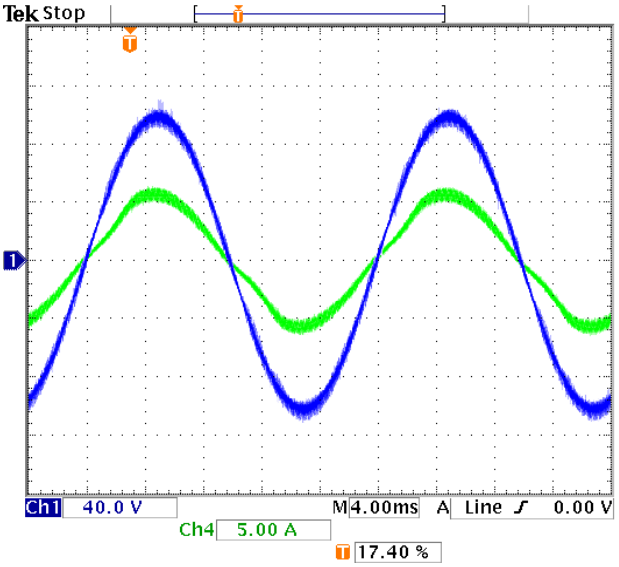

Fig. 10. Input voltage v_{ac} (Ch. 2: 20V/div, blue) and input current z_1 (Ch. 4: 5A/div, green) with series damping injection.

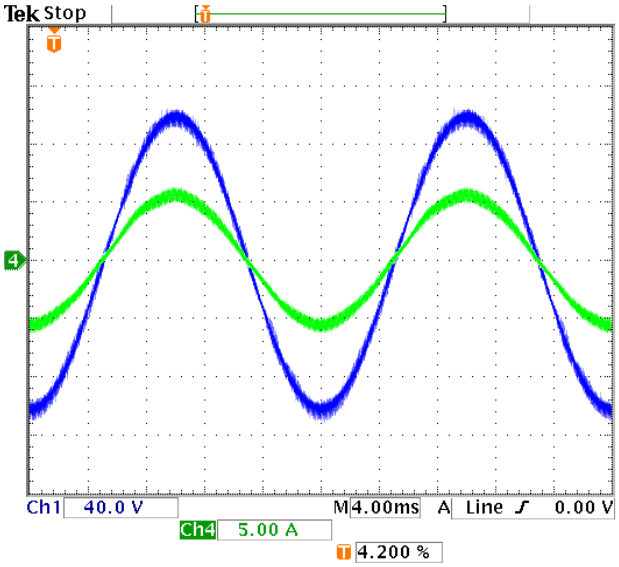

Fig. 11. Input voltage v_{ac} (Ch. 2: 20V/div, blue) and input current z_1 (Ch. 4: 5A/div, green) with series damping injection under harmonic compensation.

gain is increased the frequencies of these oscillations are increased, as well as the frequencies of the oscillations in the output voltage. However, the maximum output voltage error decreases. A look at the currents reveals that they are in phase with the current reference. However, the currents are not purely sinusoidal which is caused by model mismatch (nonlinear plant characteristics and grid harmonics). For example, the nonlinear characteristics of the diodes and transistors are not modeled. This also causes the RMS value of the output voltage and the output of the load estimator not to converge to their desired values. In steady state the maximum error of the load estimator in the experiment is approximately 4.5 % for a step change from 220 to 440 Ω.

2) Parallel Damping Injection: For this strategy the damping injection is described by (40). Increasing the value of the tuning parameter δ does not significantly influence the current waveform. Therefore, the tuning parameter value is $\delta = 0.5$. The input current z_1 and the output voltage z_2 during the load changes are shown in Fig. 7 and Fig. 9, respectively. In contrast to the series damping injection scheme the overshoot in the output voltage during load variations is less. Moreover, after a load change with parallel damping injection oscillations in the load estimator output and the output voltage are absent. For all loads the RMS value of the output voltage is higher than the desired value, but it remains within a boundary of 5%. The input current is higher than the desired current, out of phase and more distorted. An explanation for this can be found in the fact that in case of series damping injection the input current is damped to a fixed desired input current $z_1^\star$. In case of parallel damping injection the output voltage is damped to a desired output voltage trajectory ξ_2. This is a dynamic state of the controller and therefore the parallel damping injection scheme is more sensitive to modeling errors. In steady state the maximum error of the load estimator in the experiment is approximately 18 % for a load change from 220 to 440 Ω.

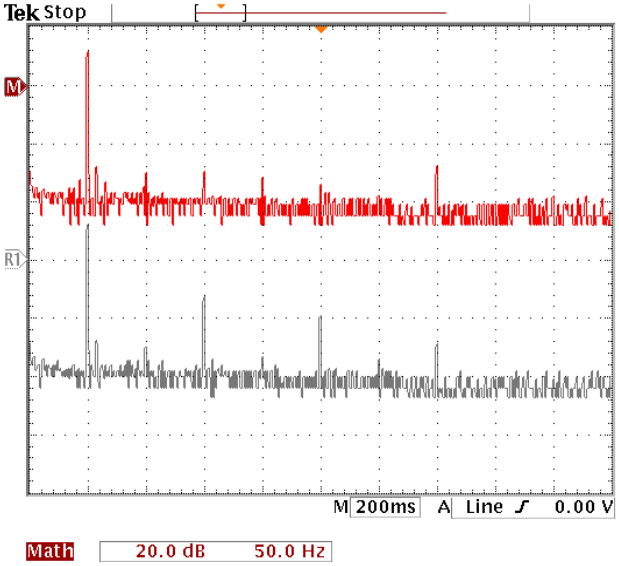

Fig. 12. Frequency spectrum of the input current z_1, with $R_\ell = 170$ Ω. (Top) Under harmonic compensation. (Bottom) Without harmonic compensation.

B. Current Shape Improvement

From the previous part it is clear that in case of series injected damping the input current waveform is more sinusoidal than in case of parallel injected damping. For further improvement of the input current waveform filter-based damping injection, introduced in Sect. V-B, is added to the series damping injection scheme.

Fig. 10 and Fig. 12 (lower) show the waveform and frequency spectrum respectively of the input current when no filter-based damping injection is used and the load is equal to 170 Ω. From the frequency spectrum it can be seen that the harmonic content of the current is dominated by the third and fifth current harmonic. To lower the total harmonic current distortion and to improve the power factor these two harmonics are compensated for. The resonant frequencies of the two

TABLE II
PARAMETER VALUES OF THE TWO DAMPING INJECTION FILTERS

Filter parameters		3rd harmonic	5th harmonic	
Resistance, R_{ih}	=	400	300	[Ω]
Inductance, L_{ih}	=	5.7	1.5	[mH]
Capacitance, C_{ih}	=	198.94	265.26	[μF]

bandpass filters coincide with the frequencies of the two current harmonics (i.e., 150 Hz and 250 Hz). The bandwidth of each filter is chosen as 2 Hz to allow small frequency deviations. These deviations are caused by the fact that in practice the fundamental frequency deviates from 50 Hz. Summarizing, the parameter values are shown in Table II.

Fig. 11 shows the resulting current waveform z_1 when the selected harmonics compensation is used, notice that the improvement of the sinusoidal shape of z_1 evidences the harmonic reduction. Indeed, Fig. 12 depicts the frequency spectrum of z_1 with and without harmonics compensation where it is clear that the third-harmonic decreases about 20 dB and fifth-harmonic decreases about 10 dB.

VII. CONCLUSION

In this paper, passivity-based controllers for the indirect stabilization of the average constant output voltage in the DC-side and unity power-factor in the ac-side for the boost full bridge converter were derived. The control objectives were achieved during the rectifier and regenerative operating mode. Particularly for the rectifier operating mode, the control scheme with series damping injection is able to reduce the error in the input current in contrast to the control scheme with parallel damping injection. If the load estimator is added to the control scheme, then the estimated load and the output voltage with the series damping injection scheme contain more oscillations during a step–wise load variation than with the parallel damping injection scheme. This is related to the fact that with parallel damping injection the output voltage error is damped. Sensitivity of the parallel damping injection scheme to modeling errors is currently being dealt with via others load estimators. For the series damping injection scheme the addition of damping injection filters results in a reduction of selected current harmonics, and thus the total harmonic input current distortion is decreased.

REFERENCES

[1] B. K. Bose, *Modern Power Electronics and A.C. Drives*, 1st ed. Prentice Hall, 2001.

[2] J. Rodriguez, J.-S. Lai, and F. Z. Peng, "Multilevel inverters: a survey of topologies, controls, and applications," *IEEE Trans. Ind. Electron.*, vol. 49, no. 4, pp. 724–738, Aug. 2002.

[3] C. Cecati, A. Dell'Aquila, M. Liserre, and V. G. Monopoli, "Design of H–bridge multilevel active rectifier for traction systems," *IEEE Trans. Ind. Appl.*, vol. 39, pp. 1541–1550, Sept./Oct. 2003.

[4] A. Dell'Aquila, M. Liserre, V. Monopoli, and P. Rotondo, "Overview of PI-based solutions for the control of DC buses of a single-phase H-bridge multilevel active rectifier," *IEEE Trans. Ind. Appl.*, vol. 44, no. 3, pp. 857 –866, May/Jun. 2008.

[5] R. Teodorescu, F. Blaabjerg, M. Liserre, and P. Loh, "Proportional-resonant controllers and filters for grid-connected voltage-source converters," *IEE Proc. Elec. Power Appl.*, vol. 153, no. 5, pp. 750–762, Sep. 2006.

[6] J. Dannehl, M. Liserre, and F. Fuchs, "Filter-based active damping of voltage source converters with LCL filter," *IEEE Trans. Ind. Electron.*, vol. 58, no. 8, pp. 3623–3633, Aug. 2011.

[7] A. Rockhill, M. Liserre, R. Teodorescu, and P. Rodriguez, "Grid-filter design for a multimegawatt medium-voltage voltage-source inverter," *IEEE Trans. Ind. Electron.*, vol. 58, no. 4, pp. 1205–1217, Apr. 2011.

[8] Y. I. Son and I. H. Kim, "Complementary PID controller to passivity-based nonlinear control of boost converters with inductor resistance," *IEEE Trans. Control Syst. Technol.*, vol. 20, no. 3, pp. 826–834, May 2012.

[9] J. R. Espinoza, G. Joós, M. Pérez, and L. A. Morán, "Stability issues in three-phase pwm current/voltage source rectifiers in the regeneration mode," in *Proc. IEEE Int. Sym. Ind. Electron. (ISIE 2000)*, 2000, pp. 453 –458.

[10] G. Escobar, D.Chevreau, R. Ortega, and E. Mendes, "An adaptive Passivity-based controller for a unity power factor rectifier," *IEEE Trans. Control Syst. Technol.*, vol. 9, no. 4, pp. 637–644, Jun. 2001.

[11] D. Karagiannis, E. Mendes, A. Astolfi, and R. Ortega, "An experimental comparison of several PWM controllers for a single–phase AC-DC converter," *IEEE Trans. Control Syst. Technol.*, vol. 11, no. 6, pp. 940–947, Nov. 2003.

[12] C. Cecati, A. Dell'Aquila, M. Liserre, and V. G. Monopoli, "A passivity-based multilevel active rectifier with adaptive compenstation for traction applications," *IEEE Trans. Ind. Appl.*, vol. 39, no. 5, pp. 1404–1412, Sep./Oct. 2003.

[13] M. M. J. de Vries, M. J. Kransse, M. Liserre, V. Monopoli, and J. M. A. Scherpen, "Passivity-based harmonic control through series/parallel damping of an H-bridge rectifier," in *Proc. IEEE Int. Sym. Ind. Electron. (ISIE 2007)*, Jun. 2007, pp. 3385 –3390.

[14] F. Giri, A. Abouloifa, I. Lachkar, and F.-Z. Chaoui, "Formal framework for nonlinear control of pwm ac/dc boost rectifiers–controller design and average performance analysis," *IEEE Trans. Control Syst. Technol.*, vol. 18, no. 2, pp. 323–335, 2010.

[15] J. M. Olm, D. Biel, M. Spinetti-Rivera, and E. Fossas, "Harmonic balance-based control of a boost DC/AC converter," *Int. J. Circ. Theor. Appl.*, 2011, DOI:10.1002/cta.755.

[16] C. Meza, D. Biel, D. Jeltsema, and J. M. A. Scherpen, "Lyapunov-based control scheme for single-phase grid-connected pv central inverters," *IEEE Trans. Control Syst. Technol.*, vol. 20, no. 2, pp. 520–529, Mar. 2012.

[17] G. Escobar, P. Mattavelli, and A. M. Stanković, "Reactive power and imbalance compensation using STATCOM with dissipativity–based control," *IEEE Trans. Control Syst. Technol.*, vol. 9, no. 5, pp. 718–727, Sep. 2001.

[18] T.-S. Lee, "Lagrangian modeling and passivity-based control of three-phase AC/DC voltage-source converters," *IEEE Trans. Ind. Electron.*, vol. 51, no. 4, pp. 892 – 902, Aug. 2004.

[19] E. Song, A. Lynch, and V. Dinavahi, "Experimental validation of nonlinear control for a voltage source converter," *IEEE Trans. Control Syst. Technol.*, vol. 17, no. 5, pp. 1135–1144, Sep. 2009.

[20] A. Gensior, H. Sira-Ramirez, J. Rudolph, and H. Guldner, "On some nonlinear current controllers for three-phase boost rectifiers," *IEEE Trans. Ind. Electron.*, vol. 56, no. 2, pp. 360 –370, Feb. 2009.

[21] M. Hernandez-Gomez, R. Ortega, F. Lamnabhi-Lagarrigue, and G. Escobar, "Adaptive PI stabilization of switched power converters," *IEEE Trans. Control Syst. Technol.*, vol. 18, no. 3, pp. 688 –698, May 2010.

[22] R. Ortega, A. Loría, P. J. Nicklasson, and H. Sira-Ramírez, *Passivity-based Control of Euler-Lagrange Systems*. Springer-Verlag, 1998.

[23] C. Batlle, A. Dòria-Cerezo, and E. Fossas, "Bidirectional power flow control of a power converter using passive hamiltonian techniques," *Int. J. Circ. Theor. Appl.*, vol. 36, no. 7, pp. 769–788, Oct. 2008.

[24] R. K. Brayton and J. K. Moser, "A theory of nonlinear networks, part I," *Quart. Appl. Math.*, vol. 12, no. 1, pp. 1–33, 1964.

[25] D. Jeltsema and J. M. A. Scherpen, "Tuning of Passivity-preserving controllers for switched-mode power converters," *IEEE Trans. Autom. Control*, vol. 49, no. 8, pp. 1333–1344, Aug. 2004.

[26] R. D. Middlebrook, "Topics in multiple-loop regulators and current-mode programming," *IEEE Trans. Power Electron.*, vol. PE-2, no. 2, pp. 109 –124, Apr. 1987.

[27] D. Jeltsema, J. M. A. Scherpen, and E. Hageman, "A robust passive power-based control strategy for three-phase voltage source rectifiers," in *Proc. IFAC World Cong.*, Prague, 2005, pp. 40–49.

[28] H. Zhou, A. Khambadkone, and X. Kong, "Passivity-based control for an interleaved current-fed full-bridge converter with a wide operating range using the Brayton-Moser form," *IEEE Trans. Power Electron.*, vol. 24, no. 9, pp. 2047 –2056, Sep. 2009.

[29] F. Blaabjerg, R. Teodorescu, M. Liserre, and A. Timbus, "Overview of control and grid synchronization for distributed power generation systems," *IEEE Trans. Ind. Electron.*, vol. 53, no. 5, pp. 1398 –1409, Oct. 2006.
[30] G. Escobar, A. Valdez, J. Leyva-Ramos, and P. Martinez, "A controller for a boost converter with harmonic reduction," *IEEE Trans. Control Syst. Technol.*, vol. 12, no. 5, pp. 717–726, Sep. 2004.
[31] D. Jeltsema, R. Ortega, and J. M. A. Scherpen, "On passivity and power-balance inequalities of nonlinear RLC circuits," *IEEE Trans. Circ. Syst. I, Fund. Theor. Appl.*, vol. 50, no. 9, pp. 1174 – 1179, Sep. 2003.
[32] R. Ortega, D. Jeltsema, and J. M. A. Scherpen, "Power shaping: a new paradigm for stabilization of nonlinear RLC circuits," *IEEE Trans. Autom. Control*, vol. 48, no. 10, pp. 1762 – 1767, Oct 2003.
[33] E. Garca-Canseco, D. Jeltsema, R. Ortega, and J. M. A. Scherpen, "Power-based control of physical systems," *Automatica*, vol. 46, no. 1, pp. 127 – 132, 2010.
[34] R. Ortega, A. J. van der Schaft, B. M. Maschke, and G. Escobar, "Interconnection and damping assignment passivity-based control of port-controlled Hamiltonian systems," *Automatica*, vol. 38, no. 4, pp. 585 – 596, 2002.
[35] M. Krstic, I. Kanellakopouslos, and P. Kokotovic, *Nonlinear and Adaptive Control Design*, 1st ed. Wiley, 1995.
[36] C. Klumpner, M. Liserre, and F. Blaabjerg, "Improved control of an active-front-end adjustable speed drive with a small de-link capacitor under real grid conditions," in *Proc. 35th IEEE Power Electron. Spec. Conf. (PESC 2004)*, vol. 2, Jun. 2004, pp. 1156 – 1162.
[37] L. Harnefors, M. Bongiorno, and S. Lundberg, "Input-admittance calculation and shaping for controlled voltage-source converters," *IEEE Trans. Ind. Electron.*, vol. 54, no. 6, pp. 3323 –3334, Dec. 2007.
[38] E. D. Sontag, "A remark on the converging-input converging-state property," *arXiv:math/0205016v1*, May 2002.
[39] Y. Gu, F. Ni, D. Yang, and H. Liu, "Switching-state phase shift method for three-phase-current reconstruction with a single DC-link current sensor," *IEEE Trans. Ind. Electron.*, vol. 58, no. 11, pp. 5186–5194, Nov. 2011.
[40] G. Escobar, P. Mattavelli, A. M. Stankovic, A. A. Valdez, and J. Leyva-Ramos, "An adaptive control for UPS to compensate unbalance and harmonic distortion using a combined capacitor/load current sensing," *IEEE Trans. Ind. Electron.*, vol. 54, no. 2, pp. 839 –847, Apr. 2007.

Dunstano del Puerto Flores (S'07-M'12) was born in Oaxaca, Mexico, in 1979. He received his M.Sc. degree in electronics engineering from the National Center for Research and Technological Development, Cuernavaca, Mexico, in 2006, and his Ph.D. degree in automatic control at the University of Groningen, The Netherlands, in 2011. In 2008 and 2009 he has been a visiting graduate scholar for a few months at the Laboratoire de Signaux et Systemes in Paris, France. In 2012 and 2013, he was with Light Controls/Nedap, The Netherlands, as an Research and Development Engineer. His research interests include nonlinear circuit theory, nonlinear control systems, power quality, energy-based modeling, and analysis and control in power electronics and power systems.

Jacquelien Scherpen (M'95-SM'03) received her M.Sc. and Ph.D. degrees in Applied Mathematics from the University of Twente, The Netherlands, in 1990 and 1994, respectively, in the field of Systems and Control. From 1994 to 2006 she was at the Delft University of Technology, The Netherlands. Since September 2006 she holds a Professor position at the University of Groningen in the Institute for Industrial Technology and Management of the faculty of Mathematics and Natural Sciences, where she was recently appointed director. She has held several visiting research positions. Her research interests include nonlinear model reduction methods, nonlinear control methods, modeling and control of physical systems with applications to electrical circuits, electro-mechanical systems and mechanical systems. Applications to smart grids are included in her interests. She has been an associate editor of the IEEE Transactions on Automatic Control, and of the International Journal of Robust and Nonlinear Control (IJRNC). Currently, she is an associate editor of the IMA Journal of Mathematical Control and Information, and she is on the editorial board of the IJRNC.

Marco Liserre , (S'00-M'02-SM'07-F13) received the MSc and PhD degree in Electrical Engineering from the Bari Polytechnic, respectively in 1998 and 2002. He has been Associate Professor at Bari Polytechnic and Professor in reliable power electronics at Aalborg University (Denmark). He is currently Full Professor and Chair of Power Electronics at Christian-Albrechts-University of Kiel (Germany). He has published 168 technical papers, 3 chapters of a book and a book (Grid Converters for Photovoltaic and Wind Power Systems,). These works have received more than 6000 citations. He has been visiting Professor at Alcala de Henares University (Spain).
He is Associate Editor of the IEEE Transactions on Industrial Electronics, IEEE Industrial Electronics Magazine, IEEE Transactions on Industrial Informatics, IEEE Transactions on power electronics and IEEE Transactions on sustainable energy. He has been Founder and Editor-in-Chief of the IEEE Industrial Electronics Magazine, Founder and Chair of the Technical Committee on Renewable Energy Systems, Co-Chairman of the ISIE 2010, and IES Vice-President responsible of the publications. He has received the IES 2009 Early Career Award, the IES 2011 Anthony J. Hornfeck Service Award and the 2011 Industrial Electronics Magazine best paper award. He is senior member of IES AdCom.

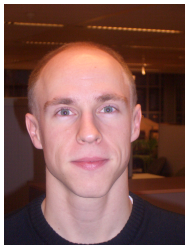

Martijn de Vries received his MSc degree in Electrical Engineering at Delft University of Technology in 2006. Part of his final thesis work was performed at the Politecnico di Bari, Italy. After receiving the degree, he was appointed for a few months at the Delft Center for Systems and Control, Delft University of Technology. During this period, he contributed to the content of Section V and VI of the paper, and to some preliminary work of the other sections.

Marco Kransse received his MSc degree in Electrical Engineering at Delft University of Technology in 2006. Part of his final thesis work was performed at the Politecnico di Bari, Italy. After receiving the degree, he was appointed for a few months at the Delft Center for Systems and Control, Delft University of Technology. During this period, he contributed to the content of Section V and VI of the paper, and to some preliminary work of the other sections.

Vito Giuseppe Monopoli (S 98) received the Laurea and Ph.D. degrees in electrical engineering from the Politecnico di Bari, Bari, Italy, in 2000 and 2004, respectively. He is currently a Research Assistant for the Converters, Electrical Machines and Drives Research Team at the Politecnico di Bari. In 2002 he received the Student Award of the ISIE conference. In 2003, he was an Invited Researcher Fellow at the School of Electrical and Electronic Engineering of the University of Nottingham (UK). His research activity concerns multilevel converters and the analysis of harmonic distortion produced by power converters and electrical drives. He is particularly interested in innovative control techniques for power converters.